BIOCHEMISTRY
including biophysical chemistry & molecular biology

Article

pubs.acs.org/biochemistry

Binuclear Cu_A Formation in Biosynthetic Models of Cu_A in Azurin Proceeds via a Novel $Cu(Cys)_2His$ Mononuclear Copper Intermediate

Saumen Chakraborty,[†,§] Michael J. Polen,[†,∥] Kelly N. Chacón,[‡,⊥] Tiffany D. Wilson,[†] Yang Yu,[†,@] Julian Reed,[†] Mark J. Nilges,[†] Ninian J. Blackburn,[*,‡] and Yi Lu[*,†]

[†]Department of Chemistry, University of Illinois at Urbana-Champaign, Urbana, Illinois 61801, United States

[‡]Institute of Environmental Health, Oregon Health & Sciences University, Portland, Oregon 97239, United States

Supporting Information

ABSTRACT: Cu_A is a binuclear electron transfer (ET) center found in cytochrome *c* oxidases (C*c*Os), nitrous oxide reductases (N_2ORs), and nitric oxide reductase (NOR). In these proteins, the Cu_A centers facilitate efficient ET (k_{ET} > 10^4 s^{-1}) under low thermodynamic driving forces (10−90 mV). While the structure and functional properties of Cu_A are well understood, a detailed mechanism of the incorporation of copper into the protein and the identity of the intermediates formed during the Cu_A maturation process are still lacking. Previous studies of the Cu_A assembly mechanism *in vitro* using a biosynthetic model Cu_A center in azurin (Cu_AAz) identified a novel intermediate X (I_x) during reconstitution of the binuclear site. However, because of the instability of I_x and the coexistence of other Cu centers, such as Cu_A' and type 1 copper centers, the identity of this intermediate could not be established. Here, we report the mechanism of Cu_A assembly using variants of Glu114XCu_AAz (X = Gly, Ala, Leu, or Gln), the backbone carbonyl of which acts as a ligand to the Cu_A site, with a major focus on characterization of the novel intermediate I_x. We show that Cu_A assembly in these variants proceeds through several types of Cu centers, such as mononuclear red type 2 Cu, the novel intermediate I_x, and blue type 1 Cu. Our results show that the backbone flexibility of the Glu114 residue is an important factor in determining the rates of T2Cu → I_x formation, suggesting that Cu_A formation is facilitated by swinging of the ligand loop, which internalizes the T2Cu capture complex to the protein interior. The kinetic data further suggest that the nature of the Glu114 side chain influences the time scales on which these intermediates are formed, the wavelengths of the absorption peaks, and how cleanly one intermediate is converted to another. Through careful understanding of these mechanisms and optimization of the conditions, we have obtained I_x in ∼80−85% population in these variants, which allowed us to employ ultraviolet−visible, electron paramagnetic resonance, and extended X-ray absorption fine structure spectroscopic techniques to identify the I_x as a mononuclear $Cu(Cys)_2(His)$ complex. Because some of the intermediates have been proposed to be involved in the assembly of native Cu_A, these results shed light on the structural features of the important intermediates and mechanism of Cu_A formation.

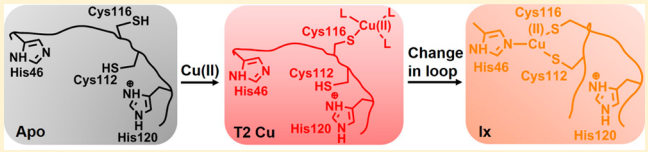

Electron transfer (ET) is essential for many biological processes, such as photosynthesis, respiration, and dinitrogen fixation.[1] To facilitate these processes, copper proteins involved in the redox and ET process, called cupredoxins, are often utilized, and they share a common Greek-key-β-barrel fold, where the majority of copper-coordinating ligands occur in a loop.[2−9] A Cys thiolate is a ligand common in cupredoxins, which makes these proteins intense in color, due to S_{Cys} → Cu charge transfer (CT) transitions. Three types of copper sites are typically found in cupredoxins: the blue mononuclear type 1 copper (T1Cu) with distorted trigonal geometry, the red mononuclear type 2 copper (T2Cu) with square pyramidal geometry, and the purple binuclear Cu_A with a diamond core geometry.[3,10−12] While the T1Cu and Cu_A sites facilitate ET, the T2Cu sites are generally involved in catalysis.[10]

One important class of these copper sites is the binuclear purple Cu_A, which is found in enzymes involved in aerobic and anaerobic respiration, such as cytochrome *c* oxidases (C*c*Os),[13−15] quinol oxidase (SoxH),[16,17] nitrous oxide reductases (N_2ORs),[18,19] and nitric oxide reductase (qCu_ANOR).[20] In these proteins, the Cu_A site acts as a terminal ET center by accepting electrons from donors, such as cytochromes *c*, and transferring them to redox partners with high efficiency (e.g., ET rate; k_{ET} > 10^4 s^{-1}), despite low thermodynamic driving forces (10−90 mV) for such ET. The Cu_A centers are characterized by a mixed valence [$Cu^{(+1.5)}$-$Cu^{(+1.5)}$] site, containing a weak Cu−Cu bond, in which one electron is delocalized between the two copper ions.[21−23] The two copper ions are coordinated by two Cys residues to form a rigid "diamond" core, and each metal ion is also coordinated by a His residue (Figure 1A). These structural features of the Cu_A site also bestow them with unique spectroscopic signatures. The ultraviolet−visible (UV−vis) spectra of Cu_A sites have two S_{Cys} → Cu(II) CTs at ∼480 and 530 nm (ε ∼ 3000−4000 M^{-1} cm^{-1}) and a broad peak due to a Cu-based ($\psi \rightarrow \psi^*$) transition

Received: June 14, 2015
Revised: September 9, 2015
Published: September 9, 2015

DOI: 10.1021/acs.biochem.5b00659
Biochemistry 2015, 54, 6071−6081

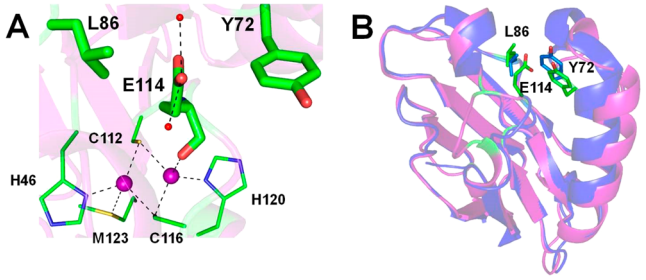

Figure 1. (A) Orientation of the Glu114 side chain in Cu_AAz between the two hydrophobic amino acids L86 and Y72, shown as sticks. Cu_A ligands are shown as lines, Cu atoms as purple spheres, and water molecules that form hydrogen bonding interactions with the Glu114 side chain as red spheres. The protein backbone is shown as a cartoon. (B) Cartoon representation of Cu_AAz (purple) and blue Cu Az (blue) showing how the placement of the Glu114 side chain in Cu_AAz sterically pushes the two helices that house L86, and Y72, compared to the blue Cu Az. Figures were generated with PyMol.

centered at ~800 nm ($\varepsilon \sim 2000\ M^{-1}\ cm^{-1}$), giving the Cu_A a strong purple color.[16,21,24−27] The electron paramagnetic resonance (EPR) spectrum consists of a seven-line hyperfine splitting pattern due to valence delocalization of the unpaired d electron between the two Cu nuclei, each having a nuclear spin $I = {}^3/_2$.[22] On the other hand, the T1Cu center also displays intense blue color, due to strong absorbance at ~600 nm ($\varepsilon \sim 2000-6000\ M^{-1}\ cm^{-1}$) that arises from the $S_{Cys}(\pi) \rightarrow Cu(II)$ CT transition. It also differs from the typical T2Cu center by a small four-line EPR hyperfine splitting pattern, which is due to valence delocalization of the unpaired d electron onto the mononuclear Cu. In general, the Cu_A center displays a hyperfine splitting ($A_z \sim 30-40 \times 10^{-4}\ cm^{-1}$) even smaller than that of T1Cu site ($A_z \sim 30-90 \times 10^{-4}\ cm^{-1}$) as the hyperfine splitting is divided into two copper atoms.[10] The red T2Cu center, in contrast, exhibits an intense absorption at ~360−400 nm, due to a $S_{Cys(\sigma)} \rightarrow Cu(II)$ CT transition. It also displays a four-line EPR hyperfine splitting pattern with a hyperfine splitting ($A_z \sim 130-180 \times 10^{-4}\ cm^{-1}$) much larger than those in Cu_A or T1Cu centers, reflecting a lower extent of covalency.[28,29] From phylogenetic and sequence analyses, it has been suggested that the blue T1Cu, red T2Cu, and purple Cu_A sites have evolved from a common ancestor.[30] All three types of Cu centers were observed in a study involving *in vitro* reconstitution of the Cu_A site of N_2OR from *Paracoccus denitrificans*.[31]

Because of the presence of multiple cofactors in the proteins containing Cu_A centers (hemes in C*c*Os and qCu_ANOR, tetranuclear Cu_Z in N_2ORs), studying the Cu_A sites in these proteins has been hindered by intense and overlapping spectral features.[16,17,19,20] One strategy that has been employed to study Cu_A sites involves expressing the soluble Cu_A domain from C*c*O and reconstituting the Cu_A site *in vitro*.[16,25−27,32−36] In a second strategy, the Cu_A ligands have been engineered in another cupredoxin protein followed by *in vitro* reconstitution of the binuclear site.[37−40] Via replacement of the Cu binding loop from T1Cu proteins with the Cu_A loop from C*c*O, the Cu_A site was successfully engineered into the CyoA domain of a copper-less quinol oxidase (called Cu_A-CyoA) and blue T1Cu proteins amicyanin (called Cu_AAmi) and azurin (Az, called Cu_AAz).[37,38,40−44]

While the Cu_A center has been well studied, one of the remaining challenges in understanding this class of copper centers is the mechanism of its formation, particularly how the mixed valence species $[Cu^{(+1.5)}\text{-}Cu^{(+1.5)}]$ is formed from either Cu(I) or Cu(II) ions. The red T2Cu Sco1 protein from the inner mitochondrial membrane, which exhibits $Cu(Cys)_2His$ ligation, has been implicated as being the chaperone responsible for delivery of Cu to the Cu_A site.[45−50] Quite interestingly, binding of both Cu(II) and Cu(I) to Sco1 has been proposed to be important for normal functioning of this protein.[51−53] Alternatively, it has been proposed that Sco1 acts as a disulfide reductase to keep the active site Cys of Cu_A in the reduced state or to maintain a proper redox buffering of metal ions. The latter inference stems from the fact that Sco1 possesses the thioredoxin fold.[50,54,55] In *Bacillus subtilis*, another protein, YpmQ, which is the yeast homologue of Sco1 and has a $Cu(Cys)_2His$ ligation, has also been proposed to be required for Cu_A assembly. Furthermore, the periplasmic protein PCu_AC, found in several prokaryotes, has been shown to deliver Cu(I) to apo Cu_A, forming the binuclear Cu(I)-Cu_A site.[54]

To gain insight into Cu_A assembly, studies have been undertaken using both the soluble domain of *Thermus thermophilus* (*Tt*) Cu_A[56,57] and biosynthetic models of Cu_A in azurin (called Cu_AAz).[58,59] A single intermediate was observed as a rapidly formed green Cu center in the soluble domain of *Tt* Cu_A, and this intermediate was identified as a mononuclear Cu(II) $(Cys)_2(His)$ complex, based on UV−vis, EPR, and X-ray absorption spectroscopy (XAS) studies.[56] On the other hand, upon addition of a 10-fold excess of $CuSO_4$ to the apo Cu_AAz, a red T2Cu intermediate was formed within 10 ms, followed by formation of the purple Cu_A site at longer times.[58] Recently, it has been shown that under subequivalent Cu(II) addition, the formation of binuclear Cu_A center is an intricate process, such that in addition to the formation of the red T2Cu intermediate, a novel green copper intermediate, I_x, and a blue T1Cu intermediate were observed prior to Cu_A formation.[59] The proposed mechanism invoked the formation of an initial red T2Cu involving Cys116 that is close to the protein exterior. The next step of the kinetic process is then branched into (a) the formation of binuclear Cu_A', a Cu_A lacking His120 ligation, and (b) a conformational change of the metal binding loop, leading to reorientation of the capture complex toward the protein interior and accompanying ligation by Cys112 and His46, forming I_x. Via comparison to the spectral properties of Cu(II)-substituted horse liver alcohol dehydrogenase (HLADH),[60−62] a Cu(II)-dithiolate complex was proposed as the identity of I_x. However, the exact ligand environment of I_x could not be established, as it was a short-lived intermediate present in a mixture with other species. The next step of the mechanism proposed the formation of a T1Cu complex from oxidation of the reduced Cu(I) product of I_x. The T1Cu complex was finally converted to the valence-delocalized Cu_A site via incorporation of *in situ* reduced Cu(I).

While the results described above are valuable, they do not fully clarify the mechanism of Cu_A formation. A critical missing piece of this mechanistic puzzle is the identity of the I_x intermediate. To identify this I_x, we examine the X-ray structure of Cu_AAz, which reveals that the side chain of Glu114, whose backbone carbonyl is very close to one of the Cu ions (2.2 Å), is positioned between two hydrophobic amino acids, Leu86 and Tyr72 (Figure 1A).[63] We thus hypothesize that the Glu114 side chain is likely more solvent-exposed in the apo form because of the negative charge on the Glu carboxylate at neutral pH. In the holo form, the coordination of the backbone carbonyl group of

DOI: 10.1021/acs.biochem.5b00659
Biochemistry 2015, 54, 6071−6081

Glu114 to one of the copper ions likely requires a specific orientation of the Glu114 side chain between the two hydrophobic amino acids. As a result of this steric effect, the helices housing these two amino acids are pushed away from each other (Figure 1B, purple). Interestingly, no such steric repulsion of the helices in blue T1Cu Az is observed (Figure 1B, blue). In contrast, the corresponding Glu side chain, found in the majority (80%) of native C*c*Os, is oriented toward the membrane interior, where it is coordinated to a Mg(II) ion.[14]

Herein, we investigate the effect of the Glu114 side chain on the sterics of the Cu binding loop and on the Cu_A assembly, by systematic substitution of this side chain with other side chains such as Gly (lacking a side chain), Ala (having a smaller, more hydrophobic methyl group), Leu (same chain length but more hydrophobic), and Gln (same chain length but with no charge). Thus, the Gly, Ala, and Leu mutations would allow us to test the effect of increasing side chain bulk, while the Leu and Gln mutations should address the role of side chain polarity in the mechanism of Cu_A formation. The specific issues we try to address in this report are (a) whether these mutations have any effect on the overall mechanism of Cu_A formation, in particular the rate of the T2Cu → I_x step of the mechanism, as this step was proposed to involve a conformational change in the metal binding loop, and (b) whether these mutations affect the formation and decay kinetics of these intermediates. Of particular interest was obtaining the I_x in higher purity compared to the original Cu_AAz and to determine its identity.

MATERIALS AND METHODS

Protein Expression and Purification. Plasmids of the Cu_AAz variants Glu114Gly/Ala/Leu/Gln containing a periplasmic leader sequence from *Pseudomonas aeruginosa* were cloned into vector pET-9a and expressed in *Escherichia coli* BL21*(DE3) (Invitrogen) competent cells. Expression and purification were conducted as described previously,[38,44,58,59] with some modifications. Bacterial cultures were grown in 2×YT medium at 25 °C until an OD of ∼0.6−1.0 was reached. Protein expression was induced with isopropyl β-D-1-thiogalactopyranoside (IPTG) (∼200 mg/2 L) and allowed to grow for 4 h. Cells were harvested and resuspended in a 20% sucrose, 1 mM ethylenediaminetetraacetic acid (EDTA), 30 mM 2-amino-2-hydroxymethylpropane-1,3-diol (Tris)·HCl solution. After centrifugation, the periplasmic membranes were lysed with an osmotic shock solution containing 4 mM NaCl and 1 mM dithiothreitol (DTT). Following centrifugation, the supernatant was treated with 500 mM NaOAc (pH 4.1) to precipitate the impurities. The solution was centrifuged one final time, and the supernatant was applied to a SP Sepharose cation exchange column (GE Healthcare) pre-equilibrated with 50 mM NH_4OAc (pH 4.1), and the protein was eluted using a shallow gradient of 50 mM NH_4OAc (pH 6.35). The fractions containing the apoprotein were pooled, pH adjusted to 6.3, and further purified with a HiTrap Q-Sepharose anion exchange column (GE Healthcare). The colorless apoprotein was then concentrated to ∼10 mL and further subjected to a size exclusion column (Sephacryl S100, GE Healthcare) to separate misfolded protein; 50 mM NH_4OAc (pH 6.35) was used as the elution buffer. The purity and the identity of the properly folded apoprotein were verified by electrospray ionization mass spectrometry. Aliquots of apoproteins were flash-frozen and stored at −80 °C until further use. Whenever required, the apoprotein was thawed, exchanged into universal buffer (UB) containing 40 mM 2-(*N*-morpholino)ethanesulfonic acid (MES), 3-(*N*-morpholino)propanesulfonic acid (MOPS), Tris, *N*-cyclohexyl-2-hydroxyl-3-aminopropanesulfonic acid (CAPS), 50 mM NaOAc, and 100 mM $NaNO_3$ at the appropriate pH using Sephadex G-25 desalting columns and concentrated to the required concentration using Amicon Ultra filtration membranes (Millipore). Protein concentrations were determined using an ε_{280} of 8440 M^{-1} cm^{-1}.

Stopped-Flow UV−Vis Absorption Spectroscopy. Stopped-flow UV−vis absorbance data were collected on an Applied Photophysics Ltd. (Leatherhead, U.K.) SX18.MV stopped-flow spectrophotometer equipped with a 256-element photodiode array detector. Equal volumes of 0.5 mM apoprotein in UB at pH 7 (UB 7) and 0.2 mM $CuSO_4$ solutions (1.0:0.4 equivalent protein:$CuSO_4$ ratio) were mixed by two syringes, and spectra were recorded over 1000 s on a logarithmic scale containing 200 data points with a sampling time of 1 ms. The final concentrations of protein and $CuSO_4$ were 0.25 and 0.1 mM, respectively. A water bath connected to the instrument was used to maintain the temperature at 15 °C. For anaerobic stopped-flow experiments, the protein and the buffer were degassed on a Schlenk line by three freeze−pump−thaw cycles. Prior to mixing, the stopped-flow instrument was washed with degassed buffer. Similarly, for O_2-rich experiments, the buffer was made O_2-saturated by being purged with O_2 for ∼15 min prior to the experiments. Raw data were subjected to global analysis using SpecFit/32 (Spectrum Software Associates, Inc.).

Global Fit Analysis of the Stopped-Flow Data. The raw stopped-flow data were processed using SpecFit/32 to deconvolute the complex spectral features and multiple kinetic processes. The data analysis is based on single-value decomposition (SVD) and nonlinear least-squares fits of the experimental data in an iterative process. During the fitting process, a set of kinetic models that seem most consistent with the experimental data were input into the software and fit globally. Using the information from the initial fitting process, the kinetic models were modified accordingly until satisfactory fit results on the basis of statistics and kinetic parameters were obtained.

Kinetic UV−Vis Absorption Spectroscopy. Kinetic UV−vis absorption data of samples containing 0.25 mM apoprotein in UB 7 and 0.1 mM $CuSO_4$ were collected while samples were constantly stirred at 10 °C on an Agilent 8453 photodiode array spectrophotometer connected with a water bath cooling system. A temperature (10 °C) lower than that (15 °C) in the stopped-flow UV−vis absorption experiment was chosen for the kinetic UV−vis absorption experiment because of concerns about the potential stability issue of the proteins at a time scale in the kinetic UV−vis absorption experiment much longer than that in the stopped-flow experiment. Because of this temperature difference, the kinetic rate constants (see Table 1) were obtained only from the stopped-flow data. For these experiments, 1000 μL of 0.5 mM apoprotein in UB 7 was taken on a 1 cm × 1 cm cuvette while the sample was being stirred and the instrument was set to collect data for 3600 s with a scan time of 0.5 s incremented by 5% after 30 s to reduce the number of data points. After a few spectra had been collected, 1000 μL of 0.2 mM $CuSO_4$ was added to the apoprotein and the cap of the cuvette was sealed with parafilm. The final concentrations of protein and $CuSO_4$ were 0.25 and 0.1 mM, respectively. After 3600 s, another experiment was started to continue for an additional 10−24 h using a longer scan time of 600 s as the later kinetic processes were slow. In other instances, similar

DOI: 10.1021/acs.biochem.5b00659
Biochemistry 2015, 54, 6071−6081

Table 1. Kinetic Models Used To Fit the Stopped-Flow Data Shown in Figure 2[a]

Cu_A variant	kinetic model	rate constants
Glu114GlyCu_AAz		k_1 = 11.28 ± 0.35 s^{-1}
		k_2 = 1.95 ± 0.03 s^{-1}
		k_3 = (0.78 ± 0.04) × 10^{-3} s^{-1}
Glu114AlaCu_AAz	$CuSO_4$ → T2Cu	k_1 = 13.52 ± 0.52 s^{-1}
	T2Cu → I_x	k_2 = 0.46 ± 0.01 s^{-1}
	I_x → T1Cu	k_3 = (1.75 ± 0.05) × 10^{-3} s^{-1}
Glu114LeuCu_AAz		k_1 = 13.12 ± 0.98 s^{-1}
		k_2 = 0.34 ± 0.01 s^{-1}
		k_3 = (1.31 ± 0.05) × 10^{-3} s^{-1}
Glu114GlnCu_AAz		k_1 = 9.36 ± 0.66 s^{-1}
		k_2 = 0.31 ± 0.01 s^{-1}
		k_3 = (2.37 ± 0.06) × 10^{-3} s^{-1}

[a]Rate constants obtained from global analysis using Specfit are shown.

experiments were performed with solutions containing equal volume of 3 mM apoprotein in UB 7 and 1.2 mM $CuSO_4$, amounting to final concentrations of 1.5 mM apoprotein and 0.6 mM $CuSO_4$. These experiments were performed at concentrations similar to those of target EPR experiments, to determine the time points at which different intermediates formed with maximal populations to characterize them by EPR. Because of the fast formation and decay of the red T2Cu intermediate (~100 ms), we focused on characterizing the later intermediates, in particular I_x, as this intermediate was not thoroughly characterized previously. From inspection of the UV−vis absorbance data from these experiments, I_x formed with a maximal population at ~50−60 s.

Electron Paramagnetic Resonance Spectroscopy. EPR data were collected using an X-band Varian E-122 spectrometer at the Illinois EPR Research Center (IERC) at 30 K using liquid He and an Air Products Helitran cryostat. Magnetic fields were calibrated with a Varian NMR Gaussmeter, while the microwave frequencies were measured with an EIP frequency counter. On the basis of the results of the kinetic UV−vis experiments, EPR samples were flash-frozen in liquid N_2 with 22% glycerol as a glassing agent at a broad range of time points after $CuSO_4$ addition. The time points were chosen to obtain as much information as possible about the discrete kinetic processes and the species present therein at that time point. The earliest time points were determined to capture the I_x in each mutant. The earliest time point (50−60 s) samples were prepared by quick mixing of equal volumes of 3 mM apoprotein in UB 7 and 1.2 mM $CuSO_4$ premixed with glycerol to give final concentrations of 1.5 mM protein and 0.6 mM $CuSO_4$. For longer time point samples (5 min to 24 h), a pool of apoprotein and $CuSO_4$ was mixed together and stirred at 10 °C while aliquots from the mixture were frozen at desired time points to monitor either the decay of I_x, the formation of T1Cu intermediate, or the formation of the final Cu_A form, after the addition of glycerol to a final concentration of 22%. All samples for longer time points had the same starting concentrations of apoprotein and $CuSO_4$ as the samples frozen at the earliest time points, to be consistent. Pure holo Cu_A forms of each variant were prepared by adding a premixed solution of 0.8 equiv of Cu(I) and 0.8 equiv of $CuSO_4$ to the apoprotein in UB 7. Substoichiometric Cu was added to ensure no excess Cu is present in solution. Cu(I) was added in the form of tetrakis(acetonitrile)copper(I) hexafluorophosphate. Experimental EPR data were simulated using SIMPOW6.[64] All the spectra were fit simultaneously to obtain relative populations and EPR parameters of various species to minimize the total root-mean-square difference (rmsd) between experimental and simulated spectra. For spin quantification, $CuSO_4$ standards were prepared at concentrations ranging from 2 to 0.0625 mM. EPR data for the standards and the protein samples were collected at a constant temperature and power of 30 K and 0.2 mW, respectively. Instrument gain was normalized across all samples. The standard curve was obtained by plotting the double integration area as a function of $CuSO_4$ concentration. The Cu(II) concentrations in protein samples were calculated from the standard curve.

X-ray Absorption Spectroscopy. The extended X-ray absorption fine structure (EXAFS) spectra were recorded at beamline X3B of the National Synchrotron Light Source with a sagittally focused Si (111) crystal monochromator. Samples were cooled to 10 K before being scanned and kept cold during data collection. Kα fluorescence was collected with a Canberra 31-element Ge detector. A Cu foil was used as a reference to calibrate energy. A 6 μm Ni filter was placed before the detector to reduce elastic scattering. Six scans of each sample were collected. These samples were prepared using a similar procedure as described in the EPR section. Samples contained 5.2−5.8 mM apoprotein in UB 7 and 2.08−2.32 mM $CuSO_4$ [1:0.4 ratio of apoprotein to Cu(II)] to a final concentration and flash-frozen in liquid N_2 at various time points (50 s to 10 h) after 20% ethylene glycol had been added as the glassing agent. For the earliest time points (50−60 s), ethylene glycol and $CuSO_4$ were premixed prior to being added to the apoprotein. Data reduction and background subtraction were performed with EXAFSPAK,[65] and data were fitted with EXCURVE 9.2.[66]

RESULTS AND DISCUSSION

Kinetics of Cu_A Reconstitution in Glu114Gly/Ala/Leu/Gln Cu_AAz. The kinetic processes of Cu_A reconstitution in Glu114Gly/Ala/Leu/Gln Cu_AAz were monitored by stopped-flow and standard UV−vis absorption spectroscopy in the presence of subequivalent amounts of $CuSO_4$. Addition of 0.4 equiv of $CuSO_4$ to 0.25 mM Glu114GlyCu_AAz led to the formation, within 100 ms, of a species displaying an intense peak at 390 nm and a weak absorption peak at ~625 nm (Figure 2A). The intense absorption centered at 390 nm is characteristic of the $S_{Cys(\sigma)}$ → Cu(II) CT transition of a red T2Cu species.[10,59] Over the next 50 s, an intermediate species formed exhibiting two intense S_{Cys} → Cu CT transitions at 413 nm (sharp) and 616 nm (broad), plus a broad peak at 762 nm. These features are similar to the previously reported intermediate X (I_x).[59] The 413 nm peak formed faster than the 616 nm peak over the next 14 min and also decayed faster. At the end of 14 min, the 413 nm peak red-shifted to 420 nm, and the 616 nm peak blue-shifted to ~610 nm, indicating the formation of blue T1Cu species. Over the next 5 h, as monitored using separate kinetic UV−vis experiments (see Materials and Methods for details), the intense absorption bands at 420 and 610 nm that can be attributed to T1Cu decayed, and the peaks for Cu_A at 478, 534, and 795 nm (Figure 2A, inset) fully developed. Unlike other variants (*vide infra*), the kinetic processes of Glu114GlyCu_AAz did not display any isosbestic point at any time point. Analysis of the stopped-flow data (1000 s) was performed using a kinetic model involving the formation of the early red T2Cu

DOI: 10.1021/acs.biochem.5b00659
Biochemistry 2015, 54, 6071−6081

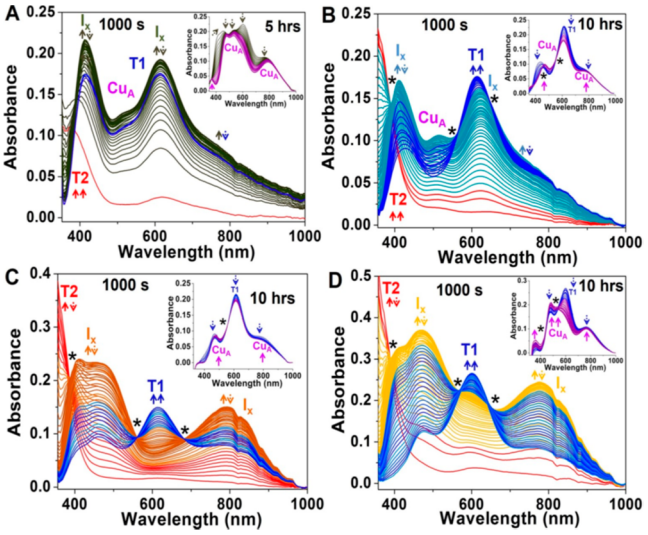

Figure 2. Stopped-flow spectra obtained after mixing 0.5 mM apo Glu114GlyCu$_A$Az (A), Glu114AlaCu$_A$Az (B), Glu114LeuCu$_A$Az (C), and Glu114GlnCu$_A$Az (D) in UB 7 buffer, with 0.2 mM $CuSO_4$. Insets show separate kinetic UV−vis experiments under the same condition, monitored for longer periods of time. Isosbestic points are denoted with asterisks. Unique UV−vis signatures for individual I_x (I_{x1} and I_{x2}) as seen by EPR (*vide infra*) cannot be deconvoluted because of spectral overlap and are labeled as I_x. Up and down arrows indicate the formation and decay of various species, respectively.

intermediate followed by the formation of I_x and the T1Cu (Figure S1 and Table 1).

Next we investigated the kinetics of incorporation of Cu into the Glu114AlaCu$_A$Az variant. Similar to the case for Glu114GlyCu$_A$Az, an early red T2Cu intermediate formed within 134 ms with an absorption band occurring at ∼362 nm (Figure 2B). A new intermediate species, corresponding to I_x, formed within the next 50 s, with intense peaks at 412 and 624 nm, and a broad feature at ∼774 nm. This process was accompanied by an isosbestic point occurring at 390 nm. The intensity of the 412 nm peak was higher than that of the 624 nm peak. A small amount of Cu$_A$ was also present. In the next ∼900 s, the 412 nm peak decreased in intensity and red-shifted to 426 nm, while the 624 nm peak blue-shifted to 616 nm, with a concomitant increase in intensity. The new features are attributed to a blue T1Cu species that developed with isosbestic conversion from I_x. The 426 and 616 nm peaks of the T1Cu intermediate decayed over the next 10 h, while absorptions in the regions typical of Cu$_A$ increased, with isosbestic points occurring at 460 and 556 nm (Figure 2B, inset). The kinetic processes within the first 1000 s were modeled (Figure S1 and Table 1) to be similar to that of Glu114GlyCu$_A$Az.

For Glu114LeuCu$_A$Az, a red T2Cu intermediate with an intense absorption peak appearing at ∼360 nm was also formed within 100 ms of mixing (Figure 2C), which decayed to I_x within 60 s with isosbestic point at 387 nm. The I_x displayed two intense absorption peaks at 413 and 470 nm and a broad feature at ∼793 nm. The intensity of the 413 nm peak was higher than that of the 470 nm peak. I_x started to decay after 85 s and was converted to a blue T1Cu intermediate with peaks occurring at 467 and 614 nm, a weak band at 793 nm, and isosbestic points at 560 and 680 nm. The T1Cu was fully formed within 40 min and started to decay to Cu$_A$ with an isosbestic point at 560 nm over 10 h (Figure 2C, inset). The stopped-flow data were modeled in the same way as those of other variants (Figure S1 and Table 1).

Finally, in Glu114GlnCu$_A$Az, a red T2Cu intermediate displaying an intense peak at ∼385 nm was observed within 100 ms of mixing (Figure 2D). Within 50 s, I_x formed displaying two intense absorption bands at 409 and 470 nm and a broad peak at ∼790 nm with an isosbestic point at 390 nm. The intensity of the 409 nm peak is slightly higher than that of the 470 nm peak. I_x decayed to a blue T1Cu intermediate with isosbestic points at 572 and 653 nm. The T1Cu intermediate having peaks at 467, 601, and ∼790 nm fully developed within 20 min. Thirty minutes from mixing, Cu$_A$ started to form, having a weak peak at ∼351 nm, two intense peaks at 479 and 541 nm, and a broad feature at ∼760 nm, formed with isosbestic points at 434 and 531 nm. Full Cu$_A$ formation was observed within 10 h (Figure 2D, inset). The kinetic processes in the first 1000 s were modeled as others (Figure S1 and Table 1).

Because no external reductant was added and the formation of the mixed valence Cu$_A$ site requires Cu(I), the reducing equivalents must be supplied by the active site cysteines. To investigate the effect of oxygen on the overall kinetic processes, we performed stopped-flow experiments under O_2-free and O_2-rich conditions. The results showed that, in the absence of O_2, no T1Cu intermediate was formed in any of the mutants, whereas under O_2-rich conditions, the rate of formation of T1Cu from I_x was faster compared to that at normal atmospheric O_2 levels (Figure S2 and Table S1). These observations suggest a role of O_2 in the formation of the T1Cu species. The absorption at ∼625 nm for I_x of Glu114Gly/Ala/Cu$_A$Az bears a strong resemblance to that of the T1Cu species that forms at latter time points. However, this peak is also present under anaerobic conditions, where the T1Cu species does not form, suggesting that this peak does indeed belong to I_x of the G and A variants.

Effect of Glu114 Substitutions on the Rates of Formation and the Characteristics of the Intermediates. It has been previously proposed that the formation of the initial capture complex for Cu ion involves Cys116 as the Cu ligand close to the exterior of the protein.[59] Our results indicate that the initial rates of formation of the red T2Cu capture complex are quite similar in all four variants (Table 1 and Figure 3A), suggesting that substitution of the Glu114 side chain has a minimal effect on the formation of the capture complex.

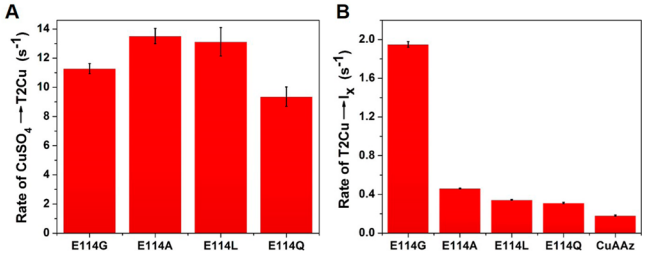

Figure 3. (A) Rates of $CuSO_4$ → T2Cu and (B) T2Cu → I_x conversion of Cu$_A$ variants obtained from the stopped-flow data. Rates in panel A are similar in all variants. In panel B, highest rate is observed for Glu114GlyCu$_A$Az, which supports the hypothesis that the T2Cu → I_x conversion involves a conformation change of the Cu$_A$ ligand loop as Gly has the most flexible backbone conformation and thus favors such a conformational change compared to the other amino acid side chains.

DOI: 10.1021/acs.biochem.5b00659
Biochemistry 2015, 54, 6071−6081

However, the rate of formation of I_x from the red T2Cu complex is fastest in Glu114GlyCu_AAz (Figure 3B and Table 1) among the four variants. In the previous study,[59] the formation of I_x from the T2Cu capture complex was proposed to involve a conformational change in the Cu_A loop, where the Cu-bound Cys116 was reoriented from the protein exterior to the interior. Our results herein support this hypothesis, as the conformational change of the Cu_A loop required for the formation of I_x would be most favorable in Glu114GlyCu_AAz, because Gly has the least steric side chain and most flexible backbone conformation in the Ramachandran plot.[67] The presence of longer side chain groups in Ala, Leu, Gln, or Glu would accordingly disfavor such a conformational change, because of steric encumbrance from these side chains and less backbone flexibility. Taken together, these results suggest that the backbone flexibility is an important factor in determining the rates of T2Cu → I_x formation. In a related study involving *Tt* Cu_A, the presence of a hydrophobic patch involving Leu155 in the metal binding loop was shown to be important in facilitating ET between cytochrome c_{552} and the *Tt* Cu_A.[68]

The kinetic data further suggest that the nature of the Glu114 side chain influences the time scales on which these intermediates are formed, the wavelengths of the absorption peaks, and how cleanly one intermediate is converted to another. For example, in Glu114GlyCu_AAz, no isosbestic point was observed during any of the kinetic processes, whereas in the other three variants, well-defined isosbestic points were observed for conversions between different species. The cleanest conversion from one intermediate to another was observed in Glu114LeuCu_AAz and Glu114GlnCu_AAz, where minimal spectral overlap among different species was present. In contrast, a strong overlap between I_x and T1Cu intermediates was observed in the other two variants. Interestingly, the split peaks for I_x at 410, and 470 nm were observed only in Glu114LeuCu_AAz and Glu114GlnCu_AAz. Additionally, the relative intensities of these two peaks are reversed in Glu114LeuCu_AAz and Glu114GlnCu_AAz, where the 410 nm peak is more intense in the former, whereas the 470 nm peak has a higher intensity in the latter variant. These observations, therefore, indicate that the Glu114 side chain plays a role in dictating the characteristics of the intermediates.

EPR Studies of the I_x Species. To further understand the nature of the intermediates, in particular, I_x, we collected X-band EPR data of two representative variants, Glu114Gly-Cu_AAz that did not display a kinetic isosbestic point and Glu114GlnCu_AAz that did. The EPR spectrum of Glu114Gly-Cu_AAz collected at 50 s (the time point at which I_x formed with a maximal population) (Figure 4a) was simulated as two mononuclear Cu(II) species in almost equal populations (38 and 46%). From the simulations, the g_z and A_z values for the two I_x intermediates were extracted to be 2.152 and 101 × 10^{-4} cm^{-1} for I_{x1} and 2.185 and 90 × 10^{-4} cm^{-1} (Table 2) for I_{x2}, respectively. While the z components of hyperfine couplings (A_z) are similar in both I_{x1} and I_{x2} that fall between those of T1Cu and T2Cu complexes, their g_z values differ significantly from each other.[10,69] A smaller g_z value in I_{x1} suggests that the strength of the thiolate−Cu interaction is slightly stronger in I_{x1} than in I_{x2}. Both g_z and A_z for I_{x1} are similar to those of the Sco protein (g_z = 2.150).[45] In addition, the A_z value is similar to that of the intermediate observed in *Tt* Cu_A (A_z = 109 × 10^{-4} cm^{-1}).[56] In both of these systems, copper is present as a bis-thiolate $Cu(Cys)_2His$ complex. By analogy, we assign I_{x1} having a similar ligand environment to these two Cu(II) centers. I_{x2} with a g_z of 2.185 is lower than most T1Cu sites (g_z ∼ 2.190−2.300).[10] I_{x2} can be best assigned as having a slightly different ligand coordination/geometry around the metal site relative to that of I_{x1}.

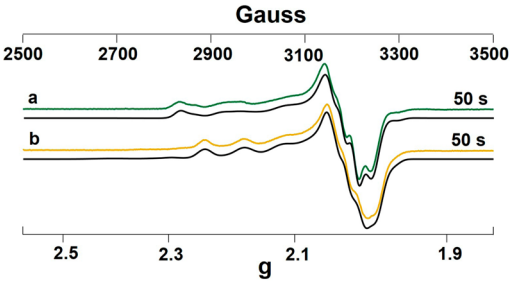

Figure 4. X-Band EPR spectra of samples containing 1.5 mM Glu114GlyCu_AAz (a) and Glu114GlnCu_AAz (b), and 0.6 mM $CuSO_4$, prepared 50 s postmixing. Experimental parameters: H = 9.053 GHz, T = 30 K, modulation = 4 G, microwave power = 0.2−0.5 mW. Simulated spectra are colored black.

For Glu114GlnCu_AAz, two mononuclear Cu(II) species were also observed at 50 s (time point at which I_x formed with a maximal population), but with unequal populations of 68 and 18% (Figure 4b). The first species has a g_z of 2.151 and an A_z of 82 × 10^{-4} cm^{-1} (Table 2), which is indicative of a species with a strong thiolate−Cu interaction and can be assigned as I_{x1} with $Cu(Cys)_2His$ ligation, using an analogy similar to that of I_{x1} of Glu114GlyCu_AAz. The second species, I_{x2}, present at an 18% population, has a g_z of 2.249 and an A_z of 133 × 10^{-4} cm^{-1}. Although the g_z and A_z values are higher than those of I_{x2} of Glu114GlyCu_AAz, these parameters are similar to those of the $Cu(Cys)_2(His)L$ (L = pyrazole or NADH) complex of HLADH (g_z = 2.200, and A_z = 115 × 10^{-4} cm^{-1}).[60−62] On the basis of this similarity, we assign I_{x2} of Glu114GlnCu_AAz as having a similar $Cu(Cys)_2(His)L$ (L = weak axial ligand) ligation/geometry.

These EPR data also suggest that a small amount of Cu_A is formed along with I_x (Table S2). Subsequently, I_x decayed and more T1Cu and Cu_A formed (see the Supporting Information). The pure Cu_A forms of each variant show the expected well-resolved seven-line hyperfine pattern, as well as the characteristic EPR parameters (Figure S3 and Table S3).

X-ray Absorption Spectroscopy. To probe the ligand and coordination environment of I_x, Cu k edge X-ray absorption spectroscopy was used. The EXAFS data for I_x of Glu114GlyCu_AAz were best simulated as two Cu−S_{Cys} ligands at 2.17 Å and one Cu−N_{His} ligand at 1.97 Å (Figure 5A and Table 3). For Glu114GlnCu_AAz, the EXAFS data (Figure 5B) for I_x were best simulated as one Cu−N_{His} ligand at 1.93 Å and two Cu−S_{Cys} ligands at 2.20 Å (Table 3). According to EPR simulation, two I_x species are present at this time point with slightly different ligand geometries (*vide supra*). However, as EXAFS measures average Cu−ligand distances, the individual Cu(II) species cannot be deconvoluted from the EXAFS data.

In I_x of these variants, the $Cu(Cys)_2His$ ligand coordination is similar to what was observed for the green intermediate in *Tt* Cu_A as well as for the Sco protein.[45,56,59] The EXAFS spectra and data analysis of the holo Cu_A samples of the Glu114XCu_AAz variants are consistent with those of other reported Cu_A systems (Figure S4 and Table S4).[56]

Proposed Mechanism of Cu_A Formation. The combined UV−vis, EPR, and EXAFS data presented in this work have allowed us to propose a mechanism of Cu_A formation in these

DOI: 10.1021/acs.biochem.5b00659
Biochemistry 2015, 54, 6071−6081

Table 2. EPR Parameters Extracted from Simulation of the Early Time Point EPR Spectra Shown in Figure 4

					population[a] (%)	
Cu_A variant		I_{x1}	I_{x2}	time	I_{x1}	I_{x2}
Glu114GlyCu_AAz	g_x	2.034	2.027	50 s	38	46
	g_y	2.044	2.020			
	g_z	2.152	2.185			
	$\|A_x\|$ ($\times 10^{-4}$ cm^{-1})	10	23			
	$\|A_y\|$ ($\times 10^{-4}$ cm^{-1})	6	22			
	$\|A_z\|$ ($\times 10^{-4}$ cm^{-1})	101	90			
Glu114Gln Cu_AAz	g_x	2.011	1.991	50 s	68	18
	g_y	2.035	2.092			
	g_z	2.151	2.249			
	$\|A_x\|$ ($\times 10^{-4}$ cm^{-1})	20	8			
	$\|A_y\|$ ($\times 10^{-4}$ cm^{-1})	14	41			
	$\|A_z\|$ ($\times 10^{-4}$ cm^{-1})	82	133			
Cu_AAz[59]	g_x		2.007			
	g_y		2.056			
	g_z		2.234			
	$\|A_x\|$ ($\times 10^{-4}$ cm^{-1})		9			
	$\|A_y\|$ ($\times 10^{-4}$ cm^{-1})		0.3			
	$\|A_z\|$ ($\times 10^{-4}$ cm^{-1})		115			
Tt Cu_A[56]	g_x	2.013				
	g_y	2.052				
	g_z	2.134				
	$\|A_x\|$ ($\times 10^{-4}$ cm^{-1})	16				
	$\|A_y\|$ ($\times 10^{-4}$ cm^{-1})	16				
	$\|A_z\|$ ($\times 10^{-4}$ cm^{-1})	109				

[a]Only I_x species present in the earliest time points are shown. See Table S2 for time-dependent populations of various species and their EPR parameters. On the basis of the higher g_z of Cu_AAz, I_x can be categorized as I_{x2s} in the variants.

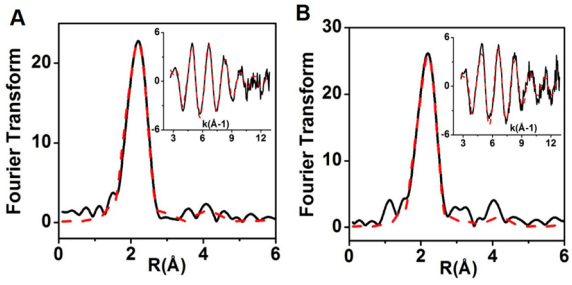

Figure 5. Fourier transform and EXAFS (inset) data of 50 s samples of Glu114GlyCu_AAz (A) and Glu114GlnCu_AAz (B). Experimental data are shown as solid black lines, and simulations are shown as dashed red lines. Parameters used to fit data are listed in Table 3.

Cu_AAz variants (Scheme 1). Upon addition of subequivalent Cu(II) to the apoproteins, an initial red T2Cu capture complex is formed within ~100 ms. Previous results from Cu_AAz established that the T2Cu capture complex is formed close to the exterior of the protein with Cys116 as the only protein-derived ligand.[44,59] The next step of the mechanism is bifurcated (Scheme 1): conversion of T2Cu to I_x and formation of a small population of Cu_A in a direct pathway from the T2Cu complex. Previously, it was hypothesized that T2Cu to I_x formation involved a conformational change of the Cu_A loop by which the capture complex is internalized from the protein exterior. Our results in this work show that T2Cu to I_x formation is fastest in Glu114GlyCu_AAz compared to those of the other mutants. As Gly has the most flexible backbone conformation, this observation, therefore, supports the hypothesis that indeed T2Cu to I_x formation is facilitated by swinging of the Cu_A loop, which brings the Cu to the protein interior.

In the next step, I_x decay and T1Cu complexes form within ~15 min. The formation of the T1Cu complex is dependent on the presence of O_2, as the T1Cu species does not form in the absence of O_2 (Figure S2). Because, in all cases, the decay of I_x is accompanied by the formation of the T1Cu species in the presence of O_2, it can be inferred that the T1Cu complex is a result of the oxidation of the decay product of I_x. EPR spin quantification shows that I_x of Glu114GlyCu_AAz decays with time (Figure S5), indicating spin loss due to the formation of the EPR silent Cu(I) species. Therefore, T1Cu is a product of the oxidation of Cu(I) formed during the decay of I_x. At an even longer time scale, the T1Cu complex decays and Cu_A starts to form (Figure 2, insets). Formation of the binuclear

Table 3. Parameters Extracted from Fitting of the EXAFS Data of I_x

		Cu−S (Cys)			Cu−N (His)			Cu−Cu[a]			
sample/fit	F	N	R (Å)	DW (Å^2)	N	R (Å^2)	DW (Å)	N	R (Å)	DW (Å^2)	E_0
Glu114GlyCu_AAz	0.53	2	2.17	0.016	1	1.97	0.02	0.15	2.412	0.0035	−0.76
Glu114GlnCu_AAz	0.60	2	2.20	0.012	1	1.93	0.005	0.1	2.340	0.005	1.52

[a]Small amounts of the binuclear Cu_A forms present at the earliest time point samples.

DOI: 10.1021/acs.biochem.5b00659
Biochemistry 2015, 54, 6071−6081

Scheme 1. Proposed Mechanism of Cu_A Formation in Glu114XCu_AAz Variants[a]

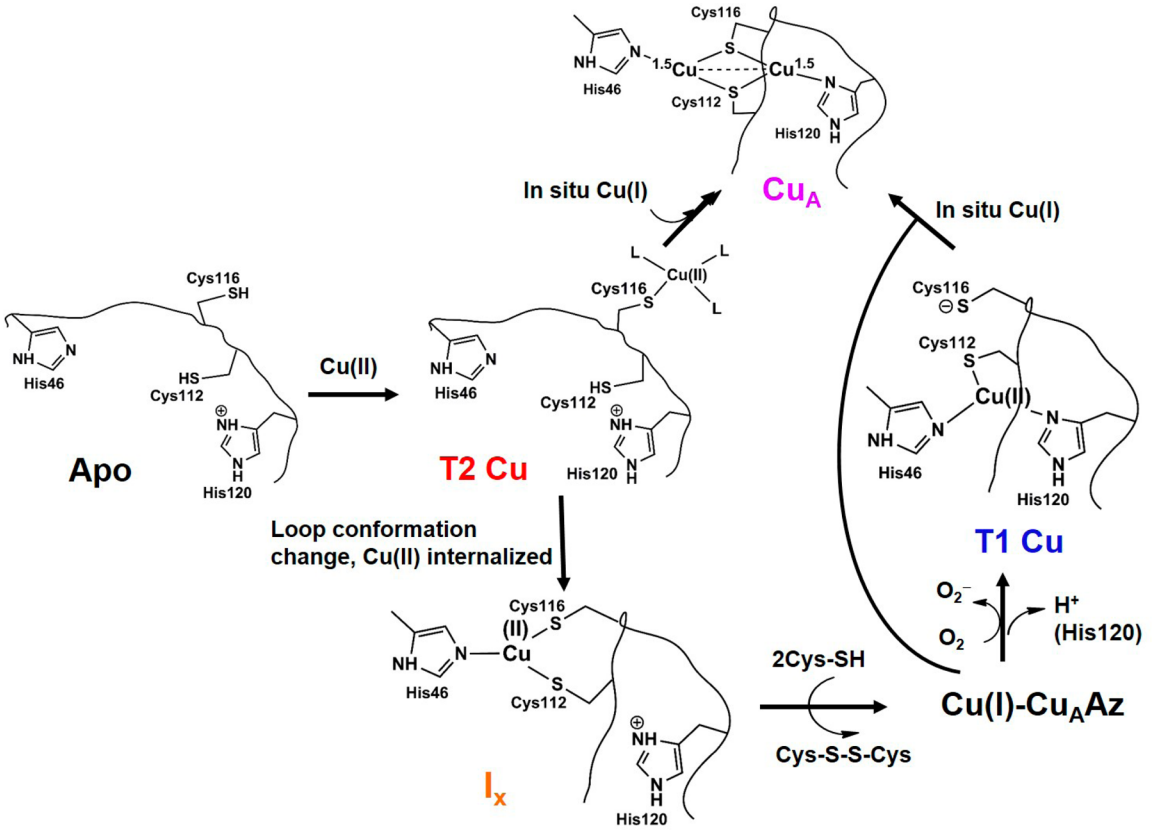

[a]The identities of the residues in the intermediates and the protonation state of His120 have not been experimentally verified for the variants and are proposed from what is known about Cu_AAz.

Cu_A from T1Cu complexes must be achieved by reaction of the T1Cu species with either free Cu(I) generated *in situ* or Cu(I) Cu_AAz.

The formation of a small population of Cu_A from T2Cu as observed here must be achieved by reaction of free Cu(I) with the Cu(II)-loaded protein. As no external reductant was added, the Cu(I) must be generated *in situ* by the reduction of Cu(II) to Cu(I) by the active site cysteines of an apo Cu_A site. As the oxidation of cysteines to cystine is a two-electron process, more than one Cu(II)-bound protein must be interacting with each other to receive the reducing equivalents from the cysteine thiols. Alternatively, Cu(I) may also be generated by the reaction of free Cu(II) with I_x, as suggested in the case of the *Tt* Cu_A system.[56] It is highly unlikely that nature uses only Cu(II) to metalate the Cu_A sites as it would be a significant waste of apoproteins to supply the reducing equivalents. Using both Cu(II) and Cu(I) would make the metalation process much more efficient as also shown in *Tt* Cu_A.[56] The yield of holo Cu_A in the Glu114XCu_AAz variants significantly increased while using a mixture of Cu(II) and Cu(I) (Table S3).

Identity of Intermediate X (I_x). A major focus of this study is to determine the ligand and coordination environment of I_x using the Glu114XCu_AAz variants. In the previous kinetic study of Cu_AAz, at the time when I_x was formed with a maximal population (~55% at ~30 s), significant populations of other types of Cu species (Cu_A' and T1Cu) were present.[59] As a result, the identity of this species could not be experimentally determined. In contrast, I_x in these Cu_A variants presented here can be obtained with a maximum of an ~80−85% combined population, with only a minor percentage of Cu_A coexisting with I_x. The electronic absorption data of the Glu114XCu_AAz variants indicate two sharp peaks in the 410−600 nm region and a broad feature at ~700−800 nm, similar to the pyrazole-substituted HLADH, which displays two peaks at ~400−500 nm, and a broad feature ~600−800 nm.[60−62] The EPR results indicate the presence of mononuclear T2Cu species with thiolate ligands. In all the variants, the EPR data suggest two mononuclear Cu complexes with minor differences in ligand coordination/geometry. Via comparison of the EPR parameters of I_{x1} to those of the green intermediate in *Tt* Cu_A and Cu(II)-Sco proteins (Table 2), the I_{x1} intermediate observed in the Glu114GlyCu_AAz and Glu114Gln Cu_AAz variants can be best described as a $Cu(Cys)_2(His)$ complex in trigonal geometry, while I_{x2} can be best described as a $Cu(Cys)_2(His)L$ (L = weak axial ligand) complex in distorted tetrahedral geometry. The proposed ligands and geometries are consistent with EXAFS data, which can be modeled as a three-coordinate mononuclear $Cu(Cys)_2$His complex. Therefore, combined UV−vis, EPR, and EXAFS data indicate the presence of Cu-bisthiolato complexes with slightly different ligation/geometry as the identity of these intermediates (Figure 6).

CONCLUSIONS

We have investigated the influence of a key Cu_A ligand (Glu114) in Cu_A assembly as well as probed the nature of intermediates formed during *in vitro* reconstitution of the Cu_A center from Cu(II) ion and apo forms of biosynthetic models in azurin (Cu_AAz). Our results show that the mechanism of Cu_A

DOI: 10.1021/acs.biochem.5b00659
Biochemistry 2015, 54, 6071−6081

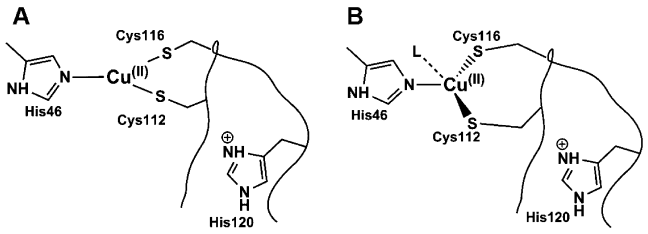

Figure 6. Schematic representation of the proposed identity of different I_x intermediates in the Cu_A variants. Two mononuclear I_x intermediates with three-coordinate $Cu(Cys)_2(His)$ ligation for I_{x1s} (A) and as a $Cu(Cys)_2(His)L$ (L= weak axial ligand) complex in distorted tetrahedral geometry for I_{x2s} (B) are proposed. Absolute residue numbering has not been experimentally assigned.

formation in variants of Glu114XCu_AAz (X = Gly, Ala, Leu, or Gln) proceeds via an initial formation of a red T2Cu center followed by another mononuclear intermediate X (I_x), then a T1Cu intermediate, and finally the binuclear Cu_A center. The results show that the Glu114 backbone flexibility is an important factor in determining the rates of T2Cu → I_x formation and suggest that Cu_A formation is facilitated by swinging of the ligand loop, which brings the external T2Cu complex to the protein interior. The kinetic data further suggest that the nature of the Glu114 side chain influences the time scales on which these intermediates are formed, the wavelengths of the absorption peaks, and how cleanly one intermediate is converted to another. This mechanistic investigation allowed us to find optimal conditions for obtaining a large population of the I_x intermediate (80−85%), facilitating the use of UV−vis, EPR, and EXAFS to elucidate the structure of I_x, which is best described as a $Cu(Cys)_2(His)$ complex in trigonal geometry. While similar intermediates and mechanisms have been identified in native Cu_A, the exact structural features and pathways for Cu_A formation are still not well understood. Our findings here of the mechanistic steps and the identification of key mononuclear intermediates during the assembly of the biosynthetic models of Cu_A in azurin and its variants have shed light on the mechanism of Cu_A formation.

■ ASSOCIATED CONTENT

Supporting Information

The Supporting Information is available free of charge on the ACS Publications website at DOI: 10.1021/acs.biochem.5b00659.

Stopped-flow data of Glu114XCu_AAz variants under O_2-rich and anaerobic conditions, full EPR parameters of all intermediates, Specfit-derived spectra of intermediates, EPR and EXAFS data of holo Glu114XCu_AAz variants, and spin quantification of Glu114GlyCu_AAz (PDF)

■ AUTHOR INFORMATION

Corresponding Authors

*E-mail: yi-lu@illinois.edu.

*E-mail: blackbni@ohsu.edu.

Present Addresses

[§]S.C.: Center for Integrated Nanotechnologies, Los Alamos National Laboratory, Los Alamos, NM 87545.

[∥]M.J.P.: Department of Chemistry, Carnegie Mellon University, Pittsburgh, PA 15213.

[⊥]K.N.C.: Department of Chemistry, Reed College, Portland, OR 97202.

[@]Y.Y.: Tianjin Institute of Industrial Biotechnology, Chinese Academy of Sciences, Tianjin, China 300308.

Funding

This work was supported by the U.S. National Science Foundation (CHE-1413328 to Y.L. and NSF Graduate Research Fellowship DGE-0925180 to K.N.C.), the U.S. National Institutes of Health (NIH) (GM054803 to N.J.B. and 5T32-GM070421 to J.R.), and the Howard Hughes Medical Institute Exceptional Research Opportunities Program (to M.J.P.). The EXAFS data were collected at beamline X3B of the National Synchrotron Light Source (NSLS) at Brookhaven National Laboratory. Beamline X3B at NSLS is operated by the Case Center for Synchrotron Biosciences, supported by NIH National Institute of Biomedical Imaging and Bioengineering Grant P30-EB-009998. NSLS is supported by the U.S. Department of Energy, Office of Science, Office of Basic Energy Sciences, under Contract DE-AC02-98CH10886.

Notes

The authors declare no competing financial interest.

■ ACKNOWLEDGMENTS

We thank Dr. Arnab Mukherjee for helpful discussions.

■ REFERENCES

(1) Liu, J., Chakraborty, S., Hosseinzadeh, P., Yu, Y., Tian, S., Petrik, I., Bhagi, A., and Lu, Y. (2014) Metalloproteins Containing Cytochrome, Iron−Sulfur, or Copper Redox Centers. *Chem. Rev. 114*, 4366−4469.

(2) Gray, H. B., Malmström, B. G., and Williams, R. J. P. (2000) Copper coordination in blue proteins. *JBIC, J. Biol. Inorg. Chem. 5*, 551.

(3) Vila, A. J., and Fernandez, C. O. (2001) Copper in Electron Transfer Proteins. In *Handbook on Metalloproteins* (Bertini, I., Sigel, A., and Sigel, H., Eds.) p 813, Marcel Dekker, New York.

(4) Wilson, T. D., Yu, Y., and Lu, Y. (2013) Understanding Copper-thiolate Containing Electron Transfer Centers by Incorporation of Unnatural Amino Acids and the CuA Center into the Type 1 Copper Protein Azurin. *Coord. Chem. Rev. 257*, 260−276.

(5) Lu, Y., Chakraborty, S., Miner, K. D., Wilson, T. D., Mukherjee, A., Yu, Y., Liu, J., and Marshall, N. M. (2013) Metalloprotein Design. In *Comprehensive Inorganic Chemistry II* (Reedijk, J., and Poeppelmeier, K., Eds.) pp 565−593, Elsevier, Amsterdam.

(6) Chakraborty, S., Hosseinzadeh, P., and Lu, Y. (2014) Metalloprotein Design and Engineering. In *Encyclopedia of Inorganic and Bioinorganic Chemistry* (Scott, R. A., Ed.) pp 1−51, John Wiley and Sons, Ltd., Chichester, U.K.

(7) Farver, O., and Pecht, I. (2008) Elucidation of Electron-Transfer Pathways in Copper and Iron Proteins by Pulse Radiolysis Experiments. In *Progress in Inorganic Chemistry*, pp 1−78, John Wiley & Sons, Inc., Chichester, U.K.

(8) Savelieff, M. G., and Lu, Y. (2010) Cu(A) centers and their biosynthetic models in azurin. *JBIC, J. Biol. Inorg. Chem. 15*, 461−483.

(9) Solomon, E. I., Heppner, D. E., Johnston, E. M., Ginsbach, J. W., Cirera, J., Qayyum, M., Kieber-Emmons, M. T., Kjaergaard, C. H., Hadt, R. G., and Tian, L. (2014) Copper active sites in biology. *Chem. Rev. 114*, 3659−3853.

(10) Lu, Y. (2004) Electron transfer: Cupredoxins. In *Biocoordination Chemistry* (Que, J. L., and Tolman, W. B., Eds.) pp 91−122, Elsevier, Oxford, U.K.

(11) Solomon, E. I. (2006) Spectroscopic Methods in Bioinorganic Chemistry: Blue to Green to Red Copper Sites. *Inorg. Chem. 45*, 8012−8025.

(12) Solomon, E. I., Xie, X., and Dey, A. (2008) Mixed valent sites in biological electron transfer. *Chem. Soc. Rev. 37*, 623−638.

DOI: 10.1021/acs.biochem.5b00659
Biochemistry 2015, 54, 6071−6081

(13) Tsukihara, T., Aoyama, H., Yamashita, E., Tomizaki, T., Yamaguchi, H., Shinzawa-Itoh, K., Nakashima, R., Yaono, R., and Yoshikawa, S. (1995) Structures of metal sites of oxidized bovine heart cytochrome c oxidase at 2.8 A. *Science (Washington, DC, U. S.) 269*, 1069−1074.
(14) Iwata, S., Ostermeier, C., Ludwig, B., and Michel, H. (1995) Structure at 2.8 A resolution of cytochrome c oxidase from Paracoccus denitrificans. *Nature 376*, 660−669.
(15) Wikstrom, M. (2004) Cytochrome c oxidase: 25 years of the elusive proton pump. *Biochim. Biophys. Acta, Bioenerg. 1655*, 241−247.
(16) Komorowski, L., Anemuller, S., and Schafer, G. (2001) First expression and characterization of a recombinant CuA-containing subunit II from an archaeal terminal oxidase complex. *J. Bioenerg. Biomembr. 33*, 27−34.
(17) Komorowski, L., and Schafer, G. (2001) Sulfocyanin and subunit II, two copper proteins with novel features, provide new insight into the archaeal SoxM oxidase supercomplex. *FEBS Lett. 487*, 351−355.
(18) Brown, K., Tegoni, M., Prudencio, M., Pereira, A. S., Besson, S., Moura, J. J., Moura, I., and Cambillau, C. (2000) A novel type of catalytic copper cluster in nitrous oxide reductase. *Nat. Struct. Biol. 7*, 191−195.
(19) Zumft, W. G., and Kroneck, P. M. H. (2006) Respiratory transformation of nitrous oxide (N2O) to dinitrogen by Bacteria and Archaea. *Adv. Microb. Physiol. 52*, 107−227.
(20) Suharti, Strampraad, M. J., Schröder, I., and de Vries, S. (2001) A Novel Copper A Containing Menaquinol NO Reductase from Bacillus azotoformans s. *Biochemistry 40*, 2632−2639.
(21) Gamelin, D. R., Randall, D. W., Hay, M. T., Houser, R. P., Mulder, T. C., Canters, G. W., de Vries, S., Tolman, W. B., Lu, Y., and Solomon, E. I. (1998) Spectroscopy of Mixed-Valence CuA-Type Centers: Ligand-Field Control of Ground-State Properties Related to Electron Transfer. *J. Am. Chem. Soc. 120*, 5246−5263.
(22) Neese, F., Zumft, W. G., Antholine, W. E., and Kroneck, P. M. H. (1996) The Purple Mixed-Valence CuA Center in Nitrous-oxide Reductase: EPR of the Copper-63-, Copper-65-, and Both Copper-65- and [15N]Histidine-Enriched Enzyme and a Molecular Orbital Interpretation. *J. Am. Chem. Soc. 118*, 8692−8699.
(23) Olsson, M. H., and Ryde, U. (2001) Geometry, reduction potential, and reorganization energy of the binuclear Cu(A) site, studied by density functional theory. *J. Am. Chem. Soc. 123*, 7866−7876.
(24) Hulse, C. L., and Averill, B. A. (1990) Isolation of a high specific activity pink, monomeric nitrous oxide reductase from Achromobacter cycloclastes. *Biochem. Biophys. Res. Commun. 166*, 729−735.
(25) Lappalainen, P., Aasa, R., Malmstrom, B. G., and Saraste, M. (1993) Soluble CuA-binding domain from the Paracoccus cytochrome c oxidase. *J. Biol. Chem. 268*, 26416−26421.
(26) Slutter, C. E., Sanders, D., Wittung, P., Malmstrom, B. G., Aasa, R., Richards, J. H., Gray, H. B., and Fee, J. A. (1996) Water-soluble, recombinant CuA-domain of the cytochrome ba3 subunit II from Thermus thermophilus. *Biochemistry 35*, 3387−3395.
(27) von Wachenfeldt, C., de Vries, S., and van der Oost, J. (1994) The CuA site of the caa3-type oxidase of Bacillus subtilis is a mixed-valence binuclear copper center. *FEBS Lett. 340*, 109−113.
(28) Lieberman, R. L., Arciero, D. M., Hooper, A. B., and Rosenzweig, A. C. (2001) Crystal Structure of a Novel Red Copper Protein from Nitrosomonas europaea. *Biochemistry 40*, 5674−5681.
(29) Arciero, D. M., Pierce, B. S., Hendrich, M. P., and Hooper, A. B. (2002) Nitrosocyanin, a red cupredoxin-like protein from Nitrosomonas europaea. *Biochemistry 41*, 1703−1709.
(30) Ryden, L. G., and Hunt, L. T. (1993) Evolution of protein complexity: the blue copper-containing oxidases and related proteins. *J. Mol. Evol. 36*, 41−66.
(31) Savelieff, M. G., Wilson, T. D., Elias, Y., Nilges, M. J., Garner, D. K., and Lu, Y. (2008) Experimental evidence for a link among cupredoxins: red, blue, and purple copper transformations in nitrous oxide reductase. *Proc. Natl. Acad. Sci. U. S. A. 105*, 7919−7924.
(32) Farrar, J. A., Lappalainen, P., Zumft, W. G., Saraste, M., and Thomson, A. J. (1995) Spectroscopic and mutagenesis studies on the CuA centre from the cytochrome-c oxidase complex of Paracoccus denitrificans. *Eur. J. Biochem. 232*, 294−303.
(33) Maneg, O., Ludwig, B., and Malatesta, F. (2003) Different Interaction Modes of Two Cytochrome-c Oxidase Soluble CuA Fragments with Their Substrates. *J. Biol. Chem. 278*, 46734−46740.
(34) Paumann, M., Lubura, B., Regelsberger, G., Feichtinger, M., Kollensberger, G., Jakopitsch, C., Furtmuller, P. G., Peschek, G. A., and Obinger, C. (2004) Soluble CuA Domain of Cyanobacterial Cytochrome c Oxidase. *J. Biol. Chem. 279*, 10293−10303.
(35) Slutter, C. E., Langen, R., Sanders, D., Lawrence, S. M., Wittung, P., Di Bilio, A. J., Hill, M. G., Fee, J. A., Richards, J. H., et al. (1996) Electron-transfer studies with the CuA domain of Thermus thermophilus cytochrome ba3. *Inorg. Chim. Acta 243*, 141−145.
(36) Williams, P. A., Blackburn, N. J., Sanders, D., Bellamy, H., Stura, E. A., Fee, J. A., and McRee, D. E. (1999) The CuA domain of Thermus thermophilus ba3-type cytochrome c oxidase at 1.6 Å resolution. *Nat. Struct. Biol. 6*, 509−516.
(37) Dennison, C., Vijgenboom, E., de Vries, S., van der Oost, J., and Canters, G. W. (1995) Introduction of a CuA site into the blue copper protein amicyanin from Thiobacillus versutus. *FEBS Lett. 365*, 92−94.
(38) Hay, M., Richards, J. H., and Lu, Y. (1996) Construction and characterization of an azurin analog for the purple copper site in cytochrome c oxidase. *Proc. Natl. Acad. Sci. U. S. A. 93*, 461.
(39) Jones, L. H., Liu, A., and Davidson, V. L. (2003) An Engineered CuA Amicyanin Capable of Intermolecular Electron Transfer Reactions. *J. Biol. Chem. 278*, 47269−47274.
(40) van der Oost, J., Lappalainen, P., Musacchio, A., Warne, A., Lemieux, L., Rumbley, J., Gennis, R. B., Aasa, R., Pascher, T., and Malmstrom, B. G. (1992) Restoration of a lost metal-binding site: construction of two different copper sites into a subunit of the E. coli cytochrome o quinol oxidase complex. *EMBO J. 11*, 3209−3217.
(41) Farver, O., Lu, Y., Ang, M. C., and Pecht, I. (1999) Enhanced rate of intramolecular electron transfer in an engineered purple CuA azurin. *Proc. Natl. Acad. Sci. U. S. A. 96*, 899−902.
(42) Hay, M. T., Ang, M. C., Gamelin, D. R., Solomon, E. I., Antholine, W. E., Ralle, M., Blackburn, N. J., Massey, P. D., Wang, X., Kwon, A. H., and Lu, Y. (1998) Spectroscopic Characterization of an Engineered Purple CuA Center in Azurin. *Inorg. Chem. 37*, 191−198.
(43) Hwang, H. J., Berry, S. M., Nilges, M. J., and Lu, Y. (2005) Axial Methionine Has Much Less Influence on Reduction Potentials in a CuA Center than in a Blue Copper Center. *J. Am. Chem. Soc. 127*, 7274−7275.
(44) Hwang, H. J., Nagraj, N., and Lu, Y. (2006) Spectroscopic Characterizations of Bridging Cysteine Ligand Variants of an Engineered Cu2(SCys)2 CuA Azurin. *Inorg. Chem. 45*, 102−107.
(45) Andruzzi, L., Nakano, M., Nilges, M. J., and Blackburn, N. J. (2005) Spectroscopic studies of metal binding and metal selectivity in Bacillus subtilis BSco, a homologue of the yeast mitochondrial protein Sco1p. *J. Am. Chem. Soc. 127*, 16548−16558.
(46) Banci, L., Bertini, I., Cavallaro, G., and Ciofi-Baffoni, S. (2011) Seeking the determinants of the elusive functions of Sco proteins. *FEBS J. 278*, 2244−2262.
(47) Horng, Y.-C., Cobine, P. A., Maxfield, A. B., Carr, H. S., and Winge, D. R. (2004) Specific copper transfer from the Cox17 metallochaperone to both Sco1 and Cox11 in the assembly of yeast cytochrome C oxidase. *J. Biol. Chem. 279*, 35334−35340.
(48) Nittis, T., George, G. N., and Winge, D. R. (2001) Yeast Sco1, a Protein Essential for Cytochrome cOxidase Function Is a Cu (I)-binding Protein. *J. Biol. Chem. 276*, 42520−42526.
(49) Balatri, E., Banci, L., Bertini, I., Cantini, F., and Ciofi-Baffoni, S. (2003) Solution structure of Sco1: a thioredoxin-like protein involved in cytochrome c oxidase assembly. *Structure 11*, 1431−1443.
(50) Banci, L., Bertini, I., Calderone, V., Ciofi-Baffoni, S., Mangani, S., Martinelli, M., Palumaa, P., and Wang, S. (2006) A hint for the function of human Sco1 from different structures. *Proc. Natl. Acad. Sci. U. S. A. 103*, 8595−8600.

DOI: 10.1021/acs.biochem.5b00659
Biochemistry 2015, 54, 6071−6081

(51) Horng, Y.-C., Leary, S. C., Cobine, P. A., Young, F. B., George, G. N., Shoubridge, E. A., and Winge, D. R. (2005) Human Sco1 and Sco2 function as copper-binding proteins. *J. Biol. Chem. 280*, 34113−34122.
(52) Siluvai, G. S., Nakano, M., Mayfield, M., and Blackburn, N. J. (2011) The essential role of the Cu (II) state of Sco in the maturation of the CuA center of cytochrome oxidase: evidence from H135Met and H135SeM variants of the Bacillus subtilis Sco. *JBIC, J. Biol. Inorg. Chem. 16*, 285−297.
(53) Siluvai, G. S., Nakano, M. M., Mayfield, M., Nilges, M. J., and Blackburn, N. J. (2009) H135A controls the redox activity of the Sco copper center. Kinetic and spectroscopic studies of the His135Ala variant of Bacillus subtilis Sco. *Biochemistry 48*, 12133−12144.
(54) Abriata, L. A., Banci, L., Bertini, I., Ciofi-Baffoni, S., Gkazonis, P., Spyroulias, G. A., Vila, A. J., and Wang, S. (2008) Mechanism of CuA assembly. *Nat. Chem. Biol. 4*, 599−601.
(55) Siluvai, G. S., Mayfield, M., Nilges, M. J., DeBeer George, S., and Blackburn, N. J. (2010) Anatomy of a red copper center: spectroscopic identification and reactivity of the copper centers of Bacillus subtilis Sco and its Cys-to-Ala variants. *J. Am. Chem. Soc. 132*, 5215−5226.
(56) Chacón, K. N., and Blackburn, N. J. (2012) Stable Cu (II) and Cu (I) mononuclear intermediates in the assembly of the CuA center of Thermus thermophilus cytochrome oxidase. *J. Am. Chem. Soc. 134*, 16401−16412.
(57) Ghosh, M. K., Basak, P., and Mazumdar, S. (2013) Mechanism of Copper Incorporation in Subunit II of Cytochrome c Oxidase from Thermus thermophilus: Identification of Intermediate Species. *Biochemistry 52*, 4620−4635.
(58) Wang, X., Ang, M. C., and Lu, Y. (1999) Kinetics of Copper Incorporation into an Engineered Purple Azurin. *J. Am. Chem. Soc. 121*, 2947−2948.
(59) Wilson, T. D., Savelieff, M. G., Nilges, M. J., Marshall, N. M., and Lu, Y. (2011) Kinetics of Copper Incorporation into a Biosynthetic Purple CuA Azurin: Characterization of Red, Blue, and a New Intermediate Species. *J. Am. Chem. Soc. 133*, 20778−20792.
(60) Farrar, J. A., Formicka, G., Zeppezauer, M., and Thomson, A. J. (1996) Magnetic and optical properties of copper-substituted alcohol dehydrogenase: a bisthiolate copper(II) complex. *Biochem. J. 317*, 447−456.
(61) Maret, W., Dietrich, H., Ruf, H.-H., and Zeppezauer, M. (1980) Active Site-Specifc Reconstituted Copper (II) Horse Liver Alcohol Dehydrogenase: A Biological Model for Type 1 Cu2+ and its Changes Upon Ligand Binding and Confnrmational Transitions. *J. Inorg. Biochem. 12*, 241−252.
(62) Maret, W., and Kozłowski, H. (1987) Electronic absorption and EPR spectroscopy of copper alcohol dehydrogenase: pink, violet and green forms at a Type 1 copper center analog. *Biochim. Biophys. Acta, Protein Struct. Mol. Enzymol. 912*, 329.
(63) Robinson, H., Ang, M. C., Gao, Y.-G., Hay, M. T., Lu, Y., and Wang, A. H. J. (1999) Structural Basis of Electron Transfer Modulation in the Purple CuA Center. *Biochemistry 38*, 5677−5683.
(64) Nilges, M. J., Matteson, K., and Belford, R. L. (2006) SIMPOW6: A software package for the simulation of ESR powder-type spectra. In *ESR Spectroscopy in Membrane Biophysics* (Hemminga, M. A., and Berliner, L., Eds.) Vol. *27*, Springer, New York.
(65) George, G. N. (1995) *EXAFSPAK*, Stanford Synchrotron Radiation Laboratory, Menlo Park, CA.
(66) Gurman, S., Binsted, N., and Ross, I. (1986) A rapid, exact, curved-wave theory for EXAFS calculations. II. The multiple-scattering contributions. *J. Phys. C: Solid State Phys. 19*, 1845.
(67) Ramachandran, G. N., Ramakrishnan, C., and Sasisekharan, V. (1963) Stereochemistry of polypeptide chain configurations. *J. Mol. Biol. 7*, 95−99.
(68) Ghosh, M. K., Rajbongshi, J., Basumatary, D., and Mazumdar, S. (2012) Role of the Surface-Exposed Leucine 155 in the Metal Ion Binding Loop of the CuA Domain of Cytochrome c Oxidase from Thermus thermophilus on the Function and Stability of the Protein. *Biochemistry 51*, 2443−2452.
(69) Solomon, E. I., Szilagyi, R. K., DeBeer George, S., and Basumallick, L. (2004) Electronic Structures of Metal Sites in Proteins and Models: Contributions to Function in Blue Copper Proteins. *Chem. Rev. 104*, 419−458.

DOI: 10.1021/acs.biochem.5b00659
Biochemistry 2015, 54, 6071−6081